INSTITUTE OF PHYSICS PUBLISHING JOURNAL OF MICROMECHANICS AND MICROENGINEERING

J. Micromech. Microeng. **13** (2003) 412–418 PII: S0960-1317(03)54541-7

Microfluidic diffusion diluter: bulging of PDMS microchannels under pressure-driven flow*

Matthew A Holden[1], Saurabh Kumar[2], Ali Beskok[2] and Paul S Cremer[1]

[1] Department of Chemistry, Texas A&M University, PO Box 30012, College Station, TX 77843–3012, USA

[2] Department of Mechanical Engineering, Texas A&M University, 3213 TAMU, College Station, TX 77843–3213, USA

E-mail: cremer@mail.chem.tamu.edu

Received 8 October 2002, in final form 28 January 2003
Published 18 March 2003
Online at stacks.iop.org/JMM/13/412

Abstract

The bulging of microfluidic systems during pressure-driven flow is potentially a major consideration for polydimethylsiloxane (PDMS)-based devices. Microchannel cross-sectional areas can change drastically as a function of flow rate and downstream microchannel position. Such geometrical flexibility leads to difficulties in predicting convective/diffusive transport for these systems. We have previously introduced a non-dimensional parameter, κ, for characterizing convection and diffusion behavior for pressure-driven flow in rigid all-glass systems. This paper describes a modification of that concept for application to non-rigid systems, which is accomplished by incorporating an experimental step to account for the bulging in PDMS/glass microsystems. Specifically, an experimental measurement of channel height by fluorescence microscopy is combined with the aforementioned theory to characterize convective/diffusive behavior at a single location in the device. This allowed the parameter κ to be determined at that point and applied to predict fluid flow in the subsequent portion of the PDMS microsystem. This procedure was applied to a PDMS/glass microfluidic diffusion dilution (μDD) device designed for generating concentration gradients. Theoretically predicted and experimentally measured distributions of concentrations within the microsystem matched well.

(Some figures in this article are in colour only in the electronic version)

1. Introduction

Polydimethylsiloxane-based microfluidics has proven to be a fast, cheap and widely accessible technology for rapid prototyping in microanalytical systems [1]. Replica molding with PDMS can be employed for making valves, pumps, electrophoretic separation systems, gradient generation as well as for many other processes [2–11]. Further PDMS advantages include optical transparency and easily modified surface chemistry [7, 11–15]. However, aspect ratio becomes a major design constraint in these systems, since very wide and shallow microchannels can easily collapse during the bonding process [17]. Though electroosmotic and vacuum-driven flow [16] through such PDMS devices can be carried out with relatively little concern for microchannel geometry changes, positive pressure-driven flow presents a unique set of challenges. Specifically, there is a serious consideration for pressure-driven flow through such microchannels, which has been largely overlooked. Namely, the pressure itself can induce a ballooning

* This work is dedicated to the memory of our friend and colleague Saurabh Kumar.

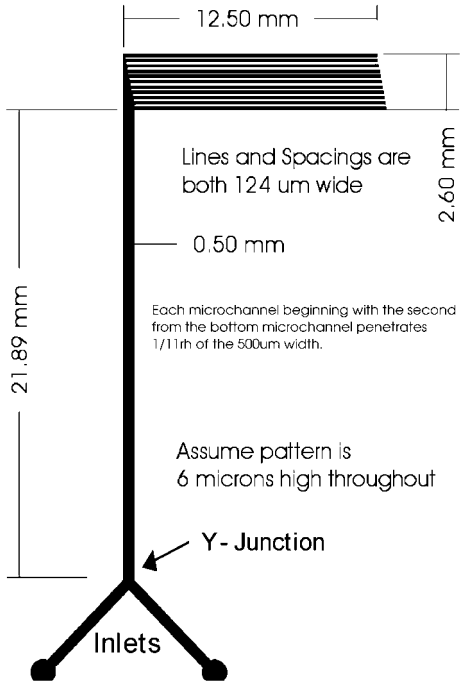

Figure 1. Schematic view of the μDD device, and its characteristic dimensions.

effect that greatly increases the cross-sectional area of the microchannel during flow. This phenomenon and its effect on creating dilution gradients is the central concern of this paper.

We have previously demonstrated a pressure-driven device for isolation of concentration gradients in a rigid, all-glass microchip [18]. The technique, called microfluidic diffusion dilution (μDD), works by combining two flowing streams at a Y-junction into a main channel, which is subsequently divided into a parallel array of microchannels (figure 1). Each channel contains a successively higher concentration of a given analyte, and the shape and distribution of the gradient formed is a function of the flow rate. Numerical simulations were successfully used to predict how the concentrations would be distributed in the microchannels. It would be convenient to extend this methodology to PDMS/glass hybrid systems, but due to the elastic nature of PDMS, the channel geometry changes as a function of flow rate. This, in turn, affects the convective/diffusive transport of analytes in the μDD.

Figure 2(a) shows a cartoon representing the main channel under conditions of pressure-driven flow. The channel would be a rectangular duct under no-flow conditions (blue rectangle in figure 2(a)); however, the cross-section takes on a hemi-cylindrical shape at high flow rates. This cross-section 'deflates' as the fluid moves downstream. Not only does the channel geometry change as a function of position, but also the channel-averaged velocity of the fluid is affected. In figure 2(a), the last segment, shown in green, represents the end of the main channel just before the microchannel entrance. When fluorescence intensities are measured here in an actual device as a function of flow rate, dramatic geometric changes can be seen. Epifluorescent data of Alexa 594 dye in buffer solution inside the main channel and channel array clearly show that the channel cross-sectional area expanded with increasing of flow rate (figure 2(b)). The bulging effect on the microchannels was not as pronounced as in the main channel because the microchannels have a higher combined cross-sectional area and lower aspect (width to height) ratios.

The work below details a modification of the previous concentration dilution theory [18] to account for cross-sectional area changes caused by the bulging of PDMS microchannels. The modification relies on a simple one-point 'calibration' method in which initial experimental data are combined with computational fluid dynamics to predict convective/diffusive transport over the entire PDMS/glass system. This allowed for good agreement to be obtained between experiment and theory.

2. Theory

The device used in these experiments had a height of 6 μm (z direction) and a main channel width of 500 μm (y direction) under no-flow conditions, yielding an aspect ratio of ~83 (figure 1). We [18] and others [19, 20] have shown that scalar transport in such high aspect ratio rectangular microchannel systems can be considered two dimensional since transverse diffusive broadening is negligible. Along the length (x direction) of the main channel, analyte transport is dominated by convective forces. By contrast, analyte transport is dominated by diffusion across the width of the main channel. Therefore, the following assumption is made:

$$\partial^2\Theta/\partial x^2 \ll \partial^2\Theta/\partial y^2 \tag{1}$$

where Θ is the non-dimensional analyte concentration, normalized by the analyte concentration at the channel inlet. Since the aspect ratio is very high, the height-averaged streamwise velocity is assumed to be uniform across the main channel width and diffusion along the channel length is negligible, so that the species transport equation can be reduced to the following form:

$$\bar{u}\frac{\partial\Theta}{\partial x} = \frac{1}{Pe}\left[\frac{\partial^2\Theta}{\partial y^2}\right] \tag{2}$$

where $\bar{u} = u_x$ is the channel-averaged fluid velocity and Pe is the Peclet number. The Peclet number is defined as

$$Pe = \frac{\bar{u}h}{\alpha} \tag{3}$$

where $\bar{u}$, h and α are the channel-averaged fluid velocity, characteristic length (width of the main channel) and the mass diffusivity, respectively. These approximations allow this system to be considered in just two dimensions (i.e., $\Theta = \Theta(x, y)$).

We have previously described a non-dimensional parameter, κ, for the characterization of convective/diffusive transport in microchannels [18]. Briefly,

$$\kappa = \frac{x}{hPe} = \frac{x\alpha}{h^2\bar{u}} \tag{4}$$

where x is the downstream distance from the Y-junction. The value of κ uniquely defines the concentration distribution $\Theta = \Theta(x, y)$ in a straight rectangular channel at any point (x) for a given channel width (h) and flow conditions (α, $\bar{u}$). Although this form of κ allowed the prediction of the

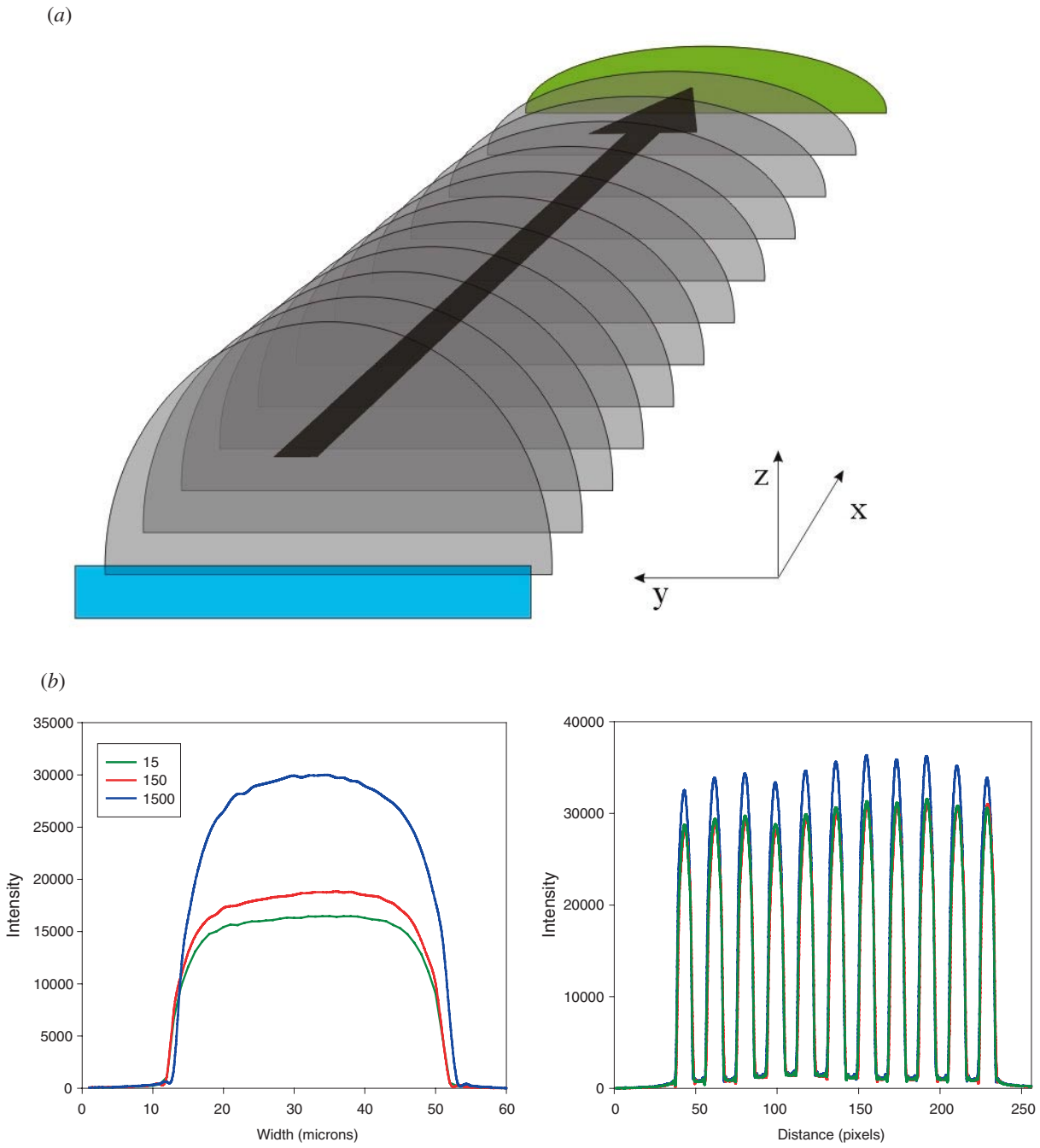

Figure 2. (*a*) Schematic representation of a bulging microchannel under pressure-driven flow (not to scale). The original geometry under no flow conditions (blue) expands greatly at high flow rates (gray). (*b*) Background subtracted fluorescence intensities taken across the width of the main channel just before the inlet to the microchannels (left) and across the microchannels (right) at various flow rates. Flow units shown in the legend are in nl min^{-1}.

concentration distribution for a rigid system, the PDMS/glass hybrid system requires an additional consideration. As stated above, under pressure-driven flow, variations in the channel cross-sectional area result in considerable changes in the channel-averaged velocity, $\bar{u}$. Hence, without knowing the cross-sectional area, the value of κ cannot be obtained for determining the theoretical concentration distribution. To remedy this, experimental data were taken to determine the cross-sectional area of the channel under a given set of flow conditions.

2.1. Experimental/computational methodology

Prior to measuring concentration gradient profiles in the μDD, both inlets were injected with the same concentration of dye. The device was then run at three flow rates and fluorescence data acquired at two positions, first at the end of the main channel just before the μDD ($x = 21$ mm), and again across the microchannels (figure 2). This measurement was critical, since the fluorescence pathlength changes at each flow rate. At our dye concentration of 6 μM, the fluorescence intensity

Table 1. Computational parameters for three flowrate cases, obtained using theory and experimental results.

Flowrate (nl min^{-1})	κ	$\bar{u}$ (m s^{-1})	$Re = \bar{u}h/\nu$	$Sc = \nu/\alpha$	$Pe = Re \times Sc$
1500	0.0059	9.24×10^{-4}	0.462	15 408	7118
150	0.026	2.09×10^{-4}	0.104	15 408	1602
15	0.12	4.52×10^{-5}	0.0225	15 408	347

was linearly related to the fluorescence pathlength, thereby allowing us to measure the channel height changes. This height information was used to correct the relative intensities when measuring the distribution of fluorophores in the concentration gradients. This was done by setting the maximum intensity for each case as $\Theta = 1$, followed by aligning each case to their respective $\Theta = 0.5$ value at the center of the main channel.

In order to measure the formation of concentration gradients, fluorescence data were obtained in the main channel at a fixed distance ($x = 21$ mm) from the Y-junction at each flow rate. Concentration curves were fitted to the experimental data, and the value of κ, which would theoretically result in the experimentally measured concentration distribution, was determined. In contrast to the rigid case [18] where κ depended only on the flow rate, here it was a function of both flow rate and channel cross-sectional area. Using equation (4), $\bar{u}$ was calculated from the volumetric flow rate. The width of the main channel was 500 μm and the diffusivity was $\alpha = 6.5 \times 10^{-11}$ m^2 s^{-1} as measured previously [18]. Using the calculated $\bar{u}$ and α, *Re* and *Pe* were determined. The values of the calculated parameters are listed in table 1 for three representative flow rates. The experimental and theoretical concentration distributions are shown in figure 3.

Transport parameters (*Re*, *Pe*), as well as experimentally determined and theoretically matched concentration distributions, were used for numerical simulations of convective/diffusive transport in the microchannel array section. The concentration distributions at the microchannel exits were calculated from the numerical solution of the incompressible Navier–Stokes and species transport equations using a spectral element algorithm [21]. Details of the computational algorithm, boundary conditions and grid independence studies are presented in [22].

3. Experimental details

3.1. Device fabrication

Standard 50 mm × 75 mm soda-lime microscope slides were spin coated with Microposit S1813 photoresist (Shipley, Marlborough, MA) to a thickness of 6 μm and baked in a convection oven at 90 °C for 1 h. The photomask was produced by reducing a negative image printed from a 1200 dpi laser printer onto Kodak technical pan photographic film (which ultimately served as the contact photomask) using a Pentax K1000 camera fitted with an SMC Pentax-A 1:2 50 mm lens. Samples were exposed using a Quintel 6000 mask aligner and developed in a 1:1 solution of Microposit developer concentrate (Microchem) and DI water. Glass barriers were glued around the photopattern and degassed PDMS was poured and cured in a convection oven at 70 °C for at least 3 h. Molds were peeled away and a piece of PDMS was sliced off to open the microchannel outlets. Using a hollow flat-tipped syringe needle, holes were reamed to form the two inlets to the device. The PDMS mold and a clean 25 mm × 50 mm microscope cover slide were simultaneously placed in a plasma cleaner and oxidized for 20 s. The two pieces were brought immediately into contact to form an irreversible bond. Water was injected as quickly as possible into an inlet port of the nascent device to hydrate the channel. This insured that the main channel did not collapse and bond with the surface during subsequent use.

3.2. Epifluorescence microscopy flow rate experiments

Fluorescence data were acquired with a Nikon E800 microscope using a Pentamax CCD camera (Princeton Instruments). The PDMS/glass device was attached to the microscope stage and two Teflon lines were inserted into the inlet ports. A modified syringe pump (Harvard Apparatus, Holliston, MA) fitted with two Hamilton 100 μl syringes, where one syringe was filled with buffer solution and the other with buffer solution plus Alexa 594 dye, pumped the fluid. Data were acquired using Metamorph (Metamorph 5.0r1, Universal Imaging Corp.) software and normalized in Sigmaplot.

4. Results and discussion

Since the bulging of the PDMS channels changed the pathlength through the dye solution, it was possible to directly determine the channel height as a function of flow rate with a constant concentration of solution. This was achieved by infusing identical concentrations of fluorophore into both inlets to the main channel. Figure 2(*b*) shows the fluorescence profile taken across the main and microchannels at various flow rates. The fluorescence intensity observed was approximately twice as high in the main channel at 1500 nl min^{-1} as at 15 nl min^{-1} despite the fact that the dye concentration remained the same everywhere in the fluid. This was a direct indication of the path length increase and, hence, channel bulging. Note that the effect of flow rate on bulging is much stronger for the main channel than the microchannels. This was due to the fact that the microchannels taken in aggregate have a greater cross-sectional area than the main channel and, therefore, the pressure was lower. Due to the constant drop in pressure as the fluid moves downstream, the force 'inflating' the microchannels is also lower than that of the main channel. Furthermore, the aspect ratio of the microchannels is significantly lower, thereby enhancing the mechanical rigidity of microchannels.

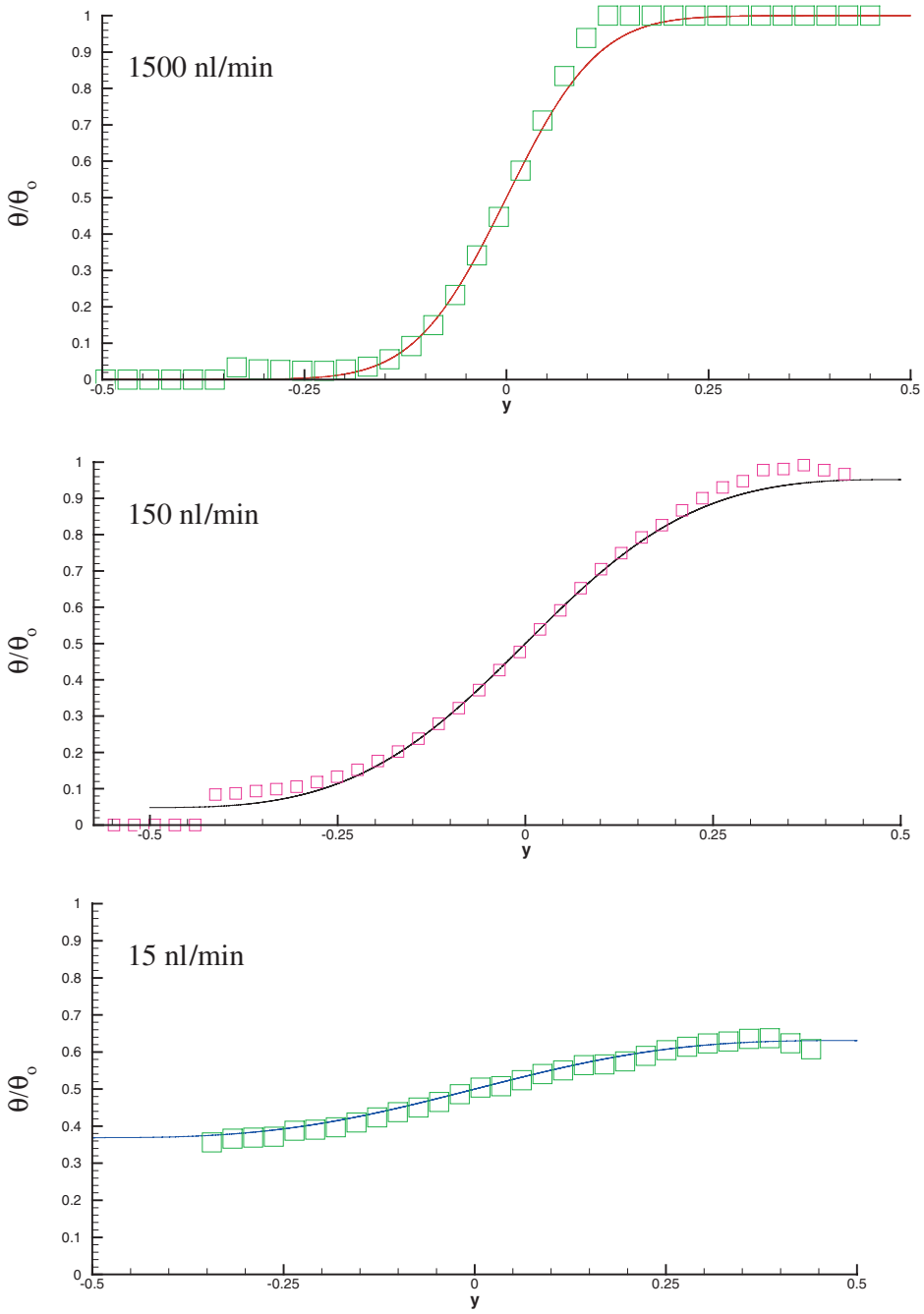

Figure 3. Normalized experimental (squares) and theoretically fitted (lines) concentration values in the main channel just before the inlet to the microchannels at various flow rates. From top to bottom flow rates were 1500, 150 and 15 nl per min.

For each flow rate, numerical simulations were performed. The concentration distribution for the 1500, 150 and 15 nl min^{-1} flow rates, as obtained both experimentally and numerically, is shown in figure 4. At 1500 nl min^{-1}, the first two microchannels had a concentration value of $\Theta = 0$. However, the last three microchannels had values around $\Theta = 1$. This demonstrates that the concentration values were not symmetric about the center microchannel, even though it was symmetric in the main channel. The asymmetry arose from the difference in convective paths of fluid particles traveling from the main channel toward the first and the last microchannels, respectively. This difference has been described previously [18]. Overall, the numerical results matched experimental results very well for all three cases.

By updating the current theory to account for channel bulging, we have demonstrated the ability to predict convective/diffusive transport in pressure-driven PDMS microchannels. This was made possible by folding a simple experimental step into the overall CFD process. Just as fluorescence intensities can be normalized by a one-point calibration, so too can microchannel behavior in flexible systems be characterized by a 'one-point' process via κ determination. By determining κ, the remaining fluid dynamic parameters can be calculated quickly.

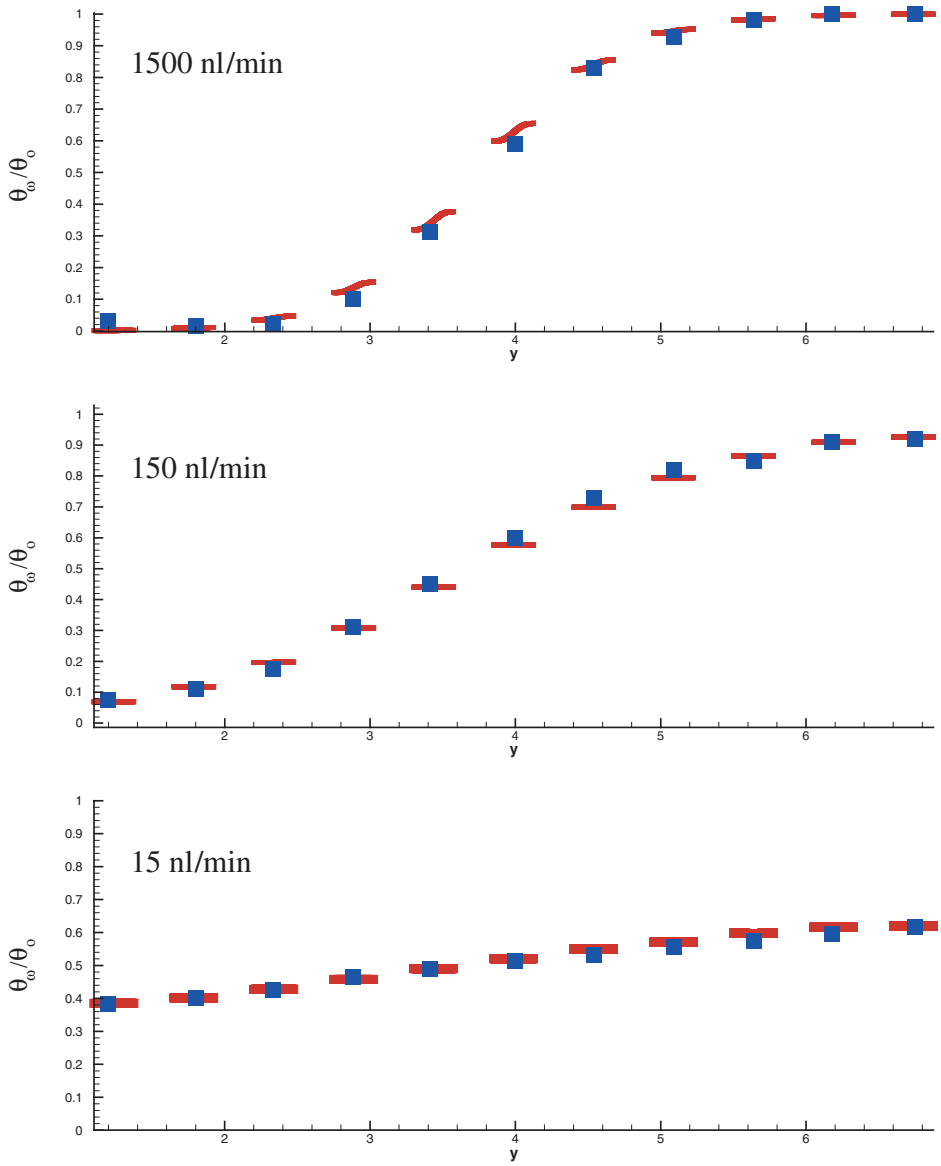

Figure 4. Normalized experimental (squares) and computationally predicted (lines) concentration values in the microchannels at various flow rates. From top to bottom flow rates were 1500, 150 and 15 nl per min.

5. Conclusions

We have build a microfluidic diffusion diluter using PDMS and performed experiments for various flow rates over two orders of magnitude. The PDMS device bulged when the flow rate was high and relaxed when it was low. The change in cross-sectional area of the device was determined experimentally and accounted for theoretically to obtain concentration gradients as a function of flow rate. This was accomplished by experimentally determining the parameter, κ, to calibrate CFD simulations.

Acknowledgments

This work was funded by an ONR-YIP Award (NOOO14-00-1-0664) and by ARO (DAAD19-01-1-0346). We would also like to acknowledge support from the Center for Integrated Microchemical Systems at Texas A&M University and the use of the TAMU/CIMS Materials Characterization Facility. PSC also gratefully acknowledges the receipt of a Beckman Young Investigator Award, and an Alfred P Sloan Fellowship and a Nontenured Faculty Award from 3M Corporation.

References

[1] Xia Y N and Whitesides G M 1998 Soft lithography *Angew. Chem. Int. Ed. Engl.* **37** 551–75

[2] Unger M A, Chou H, Thorsen T, Scherer A and Quake S R 2000 Monolithic microfabricated valves and pumps by multilayer soft lithography *Science* **288** 113–6

[3] Ocvirk G, Munroe M, Tang T, Oleschuk R, Westra K and Harrison D J 2000 Electrokinetic control of fluid flow in native poly(dimethylsiloxane) capillary electrophoresis devices *Electrophoresis* **21** 107–15

[4] Chen X X, Wu H K, Mao C D and Whitesides G M 2002 A prototype two-dimensional capillary electrophoresis system fabricated in poly(dimethylsiloxane) *Anal. Chem.* **74** 1772–8
[5] Duffy D C, Schueller O J A, Brittain S T and Whitesides G M 1999 Rapid prototyping of microfluidic switches in poly(dimethyl siloxane) and their actuation by electro-osmotic flow *J. Micromech. Microeng.* **9** 211–7
[6] Fan Z H and Harrison D J 1994 Micromachining of capillary electrophoresis injectors and separators on glass chips and evaluation of flow at capillary intersections *Anal. Chem.* **66** 177–84
[7] Mao H, Yang T and Cremer P S 2002 Design and characterization of immobilized enzymes in microfluidic systems *Anal. Chem.* **74** 379–85
[8] Jeon N L, Dertinger K W, Chiu D T, Choi I S, Stroock A D and Whitesides G M 2000 Generation of solution and surface gradients using microfluidic systems *Langmuir* **16** 8311–6
[9] Dertinger S K, Chiu D T, Jeon N L and Whitesides G M 2001 Generation of gradients having complex shapes using microfluidic networks *Anal. Chem.* **73** 1240–6
[10] Anderson J R, Chiu D T, Jackman R J, Cherniavskaya O, McDonald J C, Wu H, Whitesides S H and Whitesides G M 2000 Fabrication of topologically complex three-dimensional microfluidic systems in PDMS by rapid prototyping *Anal. Chem.* **72** 3158–64
[11] Eteshola E and Leckband D 2001 Development and characterization of an ELISA assay in PDMS microfluidic channels *Sensors Actuators* B **72** 129–33
[12] Yang T, Simanek E E and Cremer P S 2000 Creating addressable aqueous microcompartments above solid supported phospholipid bilayers using lithographically patterned poly(dimethylsiloxane) molds *Anal. Chem.* **72** 2587–9
[13] Yang T, Jung S Y, Mao H and Cremer P S 2001 Fabrication of phospholipid bilayer coated microchannels for immunoassays *Anal. Chem.* **73** 165–9
[14] Eon D, de Poucques L, Peignon M C, Cardinaud C, Turban G, Tserepi A, Cordoyiannis G, Valamontes E S, Raptis I and Gogolides E 2002 Surface modification of Si-containing polymers during etching for bilayer lithography *Microelectron. Eng.* **61–2** 901–6
[15] Abbasi F, Mirzadeh H and Katbab A A 2001 Modification of polysiloxane polymers for biomedical applications: a review *Polym. Int.* **50** 1279–87
[16] Monahan J, Gewirth A A and Nuzzo R G 2001 A method for filling complex polymeric microfluidic devices and arrays *Anal. Chem.* **73** 3193–7
[17] Delamarche E, Schmid H, Michel B and Biebuyck H 1997 Stability of molded polydimethylsiloxane microstructures *Adv. Mater.* **9** 741–6
[18] Holden M A, Kumar S, Castellana E T, Beskok A and Cremer P S Generating fixed concentration arrays in a microfluidic device *Sensors Actuators* B at press
[19] Kamholz A E and Yager P 2002 Molecular diffusive scaling laws in pressure-driven microfluidic channels; deviation from one-dimensional Einstein approximations *Sensors Actuators* B **82** 117–21
[20] Ismagilov R F, Stroock A D, Kenis P J A, Whitesides G and Stone H A 2000 Experimental and theoretical scaling laws for transverse diffusive broadening in two-phase laminar flows in microchannels *Appl. Phys. Lett.* **76** 2376–8
[21] Beskok A and Warburton T C E 2001 An unstructured hp finite-element scheme for fluid flow and heat transfer in moving domains *J. Comput. Phys.* **174** 492–509
[22] Kumar S 2002 Numerical simulation of microfluidic passive and active mixers *Masters Thesis* Mechanical Engineering, Texas A&M University, College Station, TX